Nano Research

ISSN 1998-0124 CN 11-5974/O4
https://doi.org/10.26599/NR.2026.94909312

Research Article

All-optical modulator and switcher based on 2D MgB_2 nanosheets with strong nonlinear optical response

Cong Wang[1], Xiangrong Pan[2], Jiajia Zha[3], Yichao Bai[4], Chunjiang Li[4], Kaichen Dong[4], Dan Liu[1], Shiguo Li[1], Yu Lei[4], Zhan Zhou[2], Han Zhang[5], Chaoliang Tan[3,6](✉)

[1] School of Microelectronics, Shenzhen University of Information Technology, Shenzhen 518172, China

[2] College of Chemistry and Chemical Engineering, Luoyang Normal University, Luoyang 471934, China

[3] Department of Electrical Engineering, City University of Hong Kong, Kowloon Tong, Hong Kong SAR 999077, China

[4] Institute of Materials Research, Shenzhen Key Laboratory of Advanced Layered Materials for Value-added Applications, Institute of Data and Information, Center of Double Helix, Tsinghua Shenzhen International Graduate School, Tsinghua University, Shenzhen 518055, China

[5] Collaborative Innovation Center for Optoelectronic Science & Technology, International Collaborative Laboratory of 2D Materials for Optoelectronics Science and Technology of Ministry of Education, Institute of Microscale Optoelectronics, Shenzhen University, Shenzhen 518060, China

[6] Department of Biomedical Engineering and Hong Kong Branch of National Precious Metals Material Engineering Research Center (NPMM), City University of Hong Kong, Kowloon Tong, Hong Kong SAR 999077, China

Nano Res., **Just Accepted Manuscript** • https://doi.org/10.26599/NR.2026.94909312

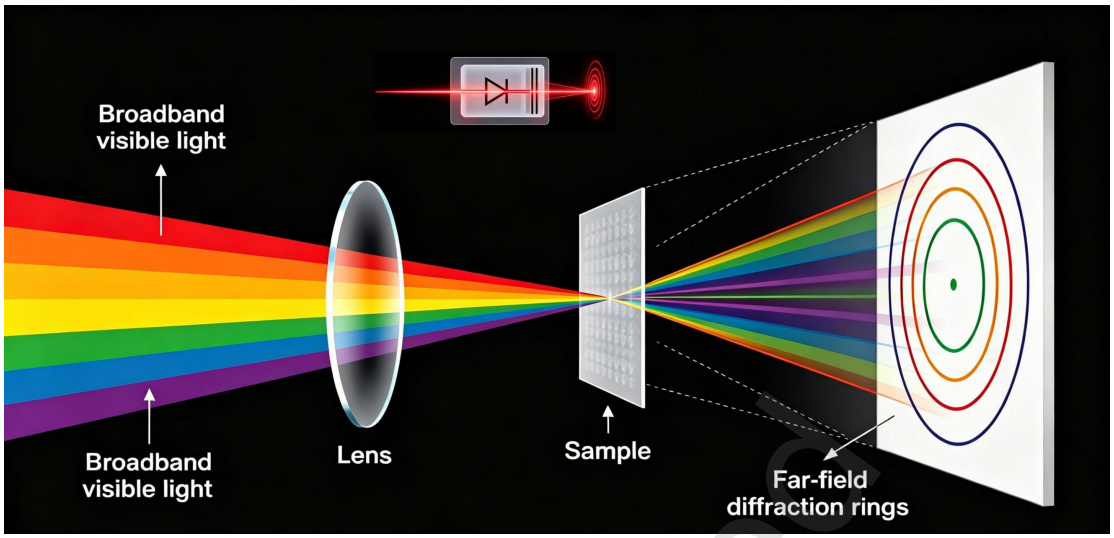
https://www.sciopen.com/journal/1998-0124 on Nov. 5, 2026

© The Authors(s)

Just Accepted

This is a "Just Accepted" manuscript, which has been examined by the peer-review process and has been accepted for publication. A "Just Accepted" manuscript is published online shortly after its acceptance,which is prior to technical editing and formatting and author proofing. Tsinghua University Press (TUP) provides "Just Accepted" as an optional and free service which allows authors to make their results available to the research community as soon as possible after acceptance. After a manuscript has been technically edited and formatted, and the page proofs have been corrected, it will be removed from the "Just Accepted" web site and published officially with volume and article number (e.g., *Nano Research*, **2025**, *18*, 94906990). Please note that technical editing may introduce minor changes to the manuscript text and/or graphics which may affect the content, and all legal disclaimers that apply to the journal pertain. In no event shall TUP be held responsible for errors or consequences arising from the use of any information contained in these "Just Accepted" manuscripts. To cite this anuscript please use its Digital Object Identifier (DOI®),which is identical for all formats of publication.

Just Accepted



All-optical switching and photonic diodes based on spatial self-phase modulation of MgB_2 nanosheets.

Just Accepted

Research Article

All-optical modulator and switcher based on 2D MgB_2 nanosheets with strong nonlinear optical response

Cong Wang [1], Xiangrong Pan [2], Jiajia Zha [3], Yichao Bai [4], Chunjiang Li [4], Kaichen Dong [4], Dan Liu [1], Shiguo Li [1], Yu Lei [4], Zhan Zhou [2], Han Zhang [5], Chaoliang Tan [3,6] ✉

[1] School of Microelectronics, Shenzhen University of Information Technology, Shenzhen 518172, China
[2] College of Chemistry and Chemical Engineering, Luoyang Normal University, Luoyang 471934, China
[3] Department of Electrical Engineering, City University of Hong Kong, Kowloon Tong, Hong Kong SAR 999077, China
[4] Institute of Materials Research, Shenzhen Key Laboratory of Advanced Layered Materials for Value-added Applications, Institute of Data and Information, Center of Double Helix, Tsinghua Shenzhen International Graduate School, Tsinghua University, Shenzhen 518055, China
[5] Collaborative Innovation Center for Optoelectronic Science & Technology, International Collaborative Laboratory of 2D Materials for Optoelectronics Science and Technology of Ministry of Education, Institute of Microscale Optoelectronics, Shenzhen University, Shenzhen 518060, China
[6] Department of Biomedical Engineering and Hong Kong Branch of National Precious Metals Material Engineering Research Center (NPMM), City University of Hong Kong, Kowloon Tong, Hong Kong SAR 999077, China

Received: 28 August 2026; **Revised: 28 October 2026**; **Accepted: 5 November 2026**

✉ Address correspondence to Chaoliang Tan, chaoltan@cityu.edu.hk

Cite this article: *Nano Research*, 2027, 20, 94909312 https://doi.org/10.26599/NR.2026.94909312

Just Accepted

Abstract

The Kerr nonlinearity in two-dimensional (2D) nanomaterials is emerging as an appealing research topic owing to their prominent light processing, modulation, and manipulation abilities. In this contribution, 2D magnesium diboride (MgB_2) nanosheets (NSs) are employed in nonlinear photonic devices based on the spatial self-phase modulation (SSPM) method. By exploiting the Kerr nonlinearity of 2D MgB_2, an all-optical phase-modulated system is proposed to realize "ON" and "OFF" states for all-optical switching. Using the same system, an optical logic gate is further demonstrated, achieving the logical "OR" operation based on 2D MgB_2 NSs dispersions. Moreover, a 2D MgB_2/BN hybrid structure is fabricated. The results show that this hybrid structure enables unidirectional nonlinear excitation, leading to spatial asymmetric light propagation. This behavior is an important prerequisite for optical diode functionality and may also provide a useful foundation for the design of optical isolators. These initial investigations suggest that 2D MgB_2 is a promising material for designing optical logic devices and represents a meaningful step toward all-optical information processing.

Just Accepted

1. Introduction

All-optical modulation has emerged as a potentially transformative strategy for photonic information processing. Compared with conventional electronic approaches, it offers intrinsically faster response times and greater immunity to electromagnetic interference[1,2]. By avoiding the inherent limitations of traditional electro-optic and opto-electronic schemes, all-optical modulation enables photon-level signal processing without intermediate electronic conversion, thereby eliminating associated speed and bandwidth bottlenecks[3,4]. In this context, nonlinear optical phenomena such as spatial self-phase modulation (SSPM) and spatial cross-phase modulation (SXPM) have garnered considerable interest, as they offer promising routes toward high-performance functional all-optical devices[3,5,6].

As typical Kerr-type nonlinear optical effects, both SSPM and SXPM arise from the light-matter interactions in nonlinear media, among which two-dimensional (2D) atomic materials have emerged as particularly promising platforms[7-13]. With the rapid expansion of the 2D material family and the increasing diversity of characterization techniques, SSPM has been widely adopted as a reliable method for evaluating nonlinear optics in emerging material systems. For instance, Ji et al. investigated the influence of gravitational fields on the SSPM response of carbon nanotubes[14], while Wu et al. extended this technique to probe the broadband nonlinear coherent behavior of graphene[15]. In another study, Wang et al. demonstrated the tunable nonlinear modulation at 632.8 nm in monolayer graphene using a similar SSPM configuration[16]. Beyond single-beam measurements, two-color-laser-based SXPM configuration has also been introduced for all-optical switching applications. A notable advance was reported by Zhao et al., who demonstrated light-controlled-light operation using monolayer MoS_2 as the interaction medium between distinct laser beams, representing an important step toward practical SXPM-based optical logic devices[5]. Despite these advances, the implementation of SSPM and SXPM techniques in 2D-material-based platforms

Just Accepted

remains at an early stage, and further systematic investigation is required to broaden their applicability in photonic systems[17-19].

MgB_2, a prototypical two-band s-wave superconductor with a critical temperature of approximately 40 K, has attracted sustained interest since its discovery[20-25]. This remarkably high transition temperature, especially for a material with a simple hexagonal lattice, has not only revitalized the search for superconductivity in non-oxide and boron-related systems but has also established MgB_2 as a benchmark for studying multi-band superconductivity. Its electronic structure features two distinct bands crossing the Fermi level: a three-dimensional π-electron band (~2 meV) and a quasi-two-dimensional σ-hole band (~7 meV), which together govern its unique superconducting dynamics[26-28]. Beyond its fundamental significance, MgB_2 is technologically attractive for superconducting electronic devices, including superconducting quantum interference devices, single-photon detectors, hot-electron bolometer mixers, and neutron detectors, owing to its long coherence length, short penetration depth, and simple binary crystal structure[29-32]. More importantly for photonic applications, MgB_2 exhibits an intrinsic nonlinear response originating from the backflow of excited quasiparticles under finite-temperature conditions [26]. It has also been demonstrated that MgB_2 can function as a saturable absorber in Yb-doped lasers to enable pulsed laser operation[33]. Given its proven capability to modulate laser pulse dynamics through saturable absorption, MgB_2 emerges as a promising candidate for extending nonlinear optical functionalities to self-phase modulation (SPM), a third-order nonlinear effect essential for all-optical signal processing.

In this work, we systematically investigate the nonlinear effect of SSPM in MgB_2 nanosheets and demonstrate their applications in all-optical switching and optical-diode-like asymmetric light propagation. Based on the Kerr nonlinearity of MgB_2, both the number and radius of the self-diffraction rings increase with the laser intensity. By analyzing the dynamic evolution of the self-diffraction ring patterns, we measure the SSPM ring-formation time and nonlinear refractive index of the

Just Accepted

nanosheets. Furthermore, we propose an all-optical switching configuration in which a visible 532 nm laser beam is controlled by a 629 nm laser beam. By exploiting the nonlinear properties of hybrid structure formed by MgB_2 nanosheets and insulating boron nitride (BN) nanosheets, asymmetric light transmission is achieved. These results highlight the potential of 2D MgB_2 for applications in all-optical information transmission and all-optical switching devices.

2. Preparation and characterization of MgB_2 nanosheets

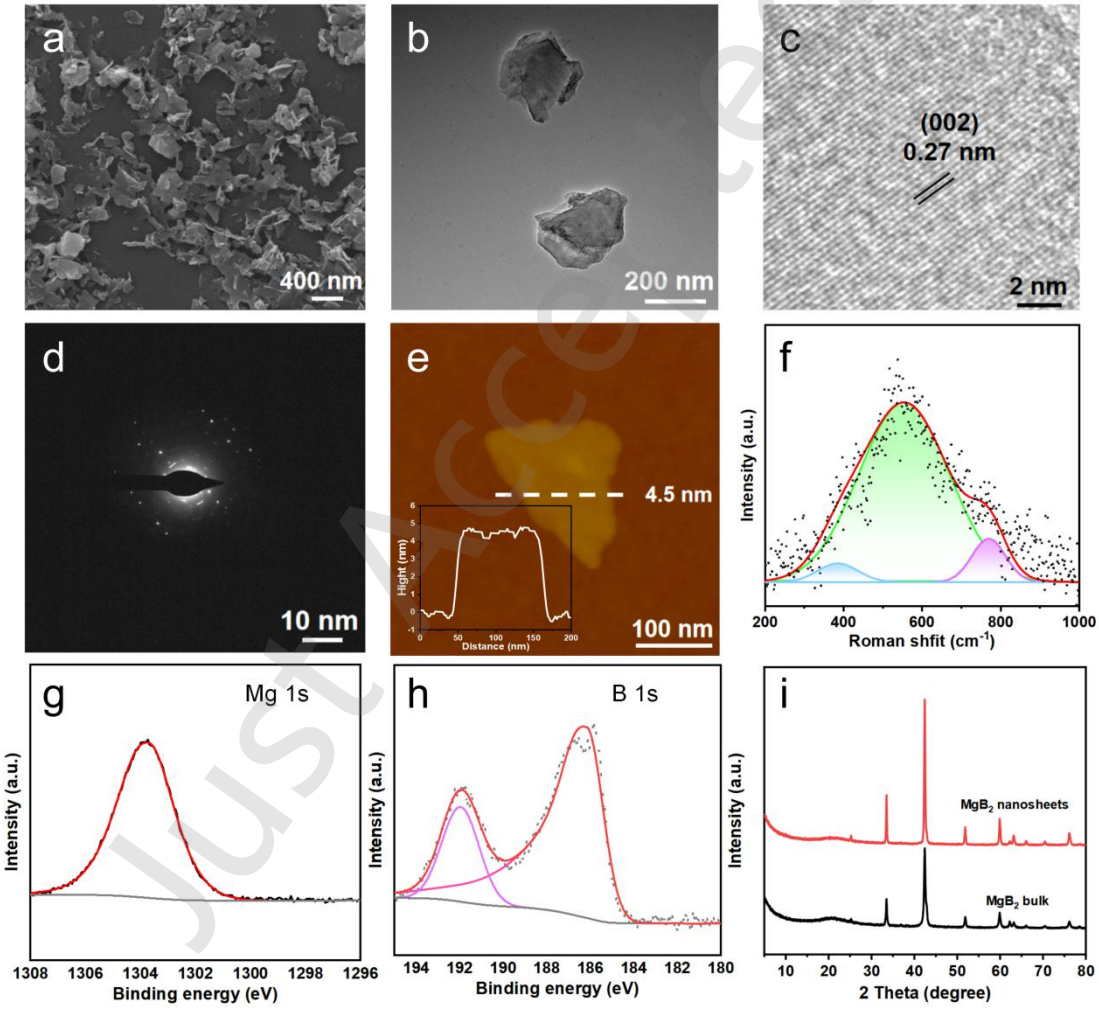


Figure 1 (a, b) Scanning electron microscopy (SEM) image and transmission electron microscopy (TEM) image of MgB_2 nanosheets, respectively. (c) High-resolution transmission electron microscopy (HRTEM) image showing the crystalline lattice structure. (d) Selected-area electron diffraction pattern of the MgB_2 nanosheets. (e) AFM image of MgB_2 nanosheets. Inset: Height profile obtained along the dashed line. (f) Raman spectrum of MgB_2 nanosheets. (g, h) XPS spectra of MgB_2 nanosheets. (i) XRD patterns of bulk MgB_2 and MgB_2 nanosheets.

MgB_2 nanosheets were prepared by a liquid-phase exfoliation method. As shown in Figure 1a and 1b, the MgB_2 nanosheets are successfully exfoliated, exhibiting a

Just Accepted

lateral size of ~200 nm. The lattice fringes with a spacing of 0.27 nm in Figure 1c can be assigned to the (002) planes of MgB_2 nanosheets. The selected-area electron diffraction (SAED) pattern (Figure 1d) indicates that the nanosheets retain good crystallinity after exfoliation. The atomic force microscopy (AFM) was used to further characterize the morphology and thickness of the fabricated MgB_2 nanosheets (Figure 1e). The measured thickness is approximately 4.5 nm, suggesting the formation of few-layer nanosheets. The Raman spectrum displays a characteristic peak at 550 cm^{-1} (Figure 1f), confirming the successful preparation of MgB_2 nanosheets, which agrees well with previously reported results[34]. In addition, X-ray photoelectron spectroscopy (XPS) was performed to evaluate the elemental composition and chemical states, as shown in Figure 1g and 1h. The Mg 1s and B 1s peaks are consistent with those reported in previous studies[35]. The B 1s spectrum can be deconvoluted into two peaks centered at 186.6 eV and 192 eV, which are ascribed to B–B and B–O bonds, respectively. Furthermore, the X-ray diffraction (XRD) pattern of the MgB_2 nanosheets (Figure 1i) is consistent with that of bulk MgB_2, further confirming the preservation of the MgB_2 crystal structure after exfoliation.

3. Experimental results

3.1 SSPM experimental setup

The SSPM experimental setup is illustrated in Figure 2a, which is used to evaluate the nonlinear optical response of the MgB_2 nanosheets. Lasers with wavelengths of 532 nm and 629 nm were employed in the experiment as excitation sources to interact with the dispersed nanosheet sample. After passing through a lens with a focal length of 200 mm, the laser beam was focused onto the sample. The sample was contained in a 10 mm optical cuvette and consisted of MgB_2 nanosheets dispersed in N,N-Dimethylformamide (DMF). The resulting diffraction ring patterns were recorded using a CMOS camera. The SSPM-based nonlinear optical response of the MgB_2 nanosheets originated from their Kerr nonlinearity.

3.2 Nonlinear Kerr effect

Just Accepted

The Kerr effect provides a fundamental basis for investigating the nonlinear optical properties of 2D materials. Specifically, the intensity-dependent refractive index can be expressed according to the nonlinear Kerr effect as $n = n_0 + n_2 I$, where n_0 is the linear refractive index of the solvent and n_2 is the nonlinear refractive index of the 2D material. When a laser beam propagates through a dispersion containing exfoliated 2D nanosheets, the intensity-dependent refractive index induces a spatially varying phase shift, which leads to nonlinear modulation of the transverse intensity distribution of the transmitted beam. This phase shift can be described as[7,10,11],

$$\Delta\varphi = \frac{2\pi n_0}{\lambda}\int_0^{L_{eff}} n_2 I(r,z)dz,$$

Where λ is the wavelength of the incident laser, L_{eff} is the effective optical length of the dispersion medium, and $I(r, z)$ represents the optical intensity distribution along the radial coordinate r and propagation direction z. The phase shift $\Delta\varphi$ is related to the spatial intensity profile of the incident laser beam. For two radial positions, r_1 and r_2 on the Gaussian beam profile, the slope $(\Delta\varphi/\mathrm{dr})_{r1}$ and $(\Delta\varphi/\mathrm{dr})_{r2}$ are the same. The emergence of concentric diffraction patterns is dictated by a specific criterion, which can be expressed as follows in the context of SSPM. $\Delta\varphi_{(r_1)} - \Delta\varphi_{(r_2)} = 2N\pi$, where N is an integer. The dark and bright rings correspond to odd and even values of N, respectively. Based on this relationship, the nonlinear refractive index n_2 can be written as:

$$n_2 = \frac{\lambda}{2n_0 L_{eff}} \cdot \frac{N}{I},$$

where λ, n_0, and L_{eff} denote the incident wavelength, linear refractive index, and effective optical thickness, respectively. The nonlinear optical response $R = N/I$ is determined from the diffraction ring number. The third nonlinear susceptibility $\chi^{(3)}_{total}$ can be calculated from the nonlinear refractive index using

$$\chi^{(3)}_{total} = \frac{cn_0^2}{12\pi^2} 10^{-7} n_2 \ (e.s.u)$$

3.3 SSPM diffraction pattern formation

In SSPM, the formation of diffraction ring patterns can be explained by the wind chime model[5]. In this model, each 2D nanosheet is regarded as an independent unit

Just Accepted

randomly dispersed in the solution. Upon irradiation by the incident laser beam, the 2D nanosheets are polarized and subsequently tend to align in the direction of the laser-induced electric field. This alignment process is driven by energy relaxation of the incident laser beam. When all the domains reach a consistent state, nonlocal electronic coherence is established, leading to the formation of the maximum number of diffraction rings. Figure 2b and 2c show the temporal evolution of the diffraction ring patterns under continuous-wave laser excitation at wavelengths of 532 nm and 629 nm, respectively. The diffraction rings remain nearly symmetric within the first 0.2 s and then gradually become asymmetric after 0.2 s. This asymmetry originates from the non-axisymmetric thermal convection induced by the photothermal effect. This diffraction-ring collapse phenomenon can be addressed by fabricating the thin-film structure[17], changing the light-material interaction mode[16,36,37], and exploring new materials[8], which will reduce the influence of photothermal effects on the diffraction rings. At relatively low input powers, thermal convection and conduction contribute comparably to heat transport. As the laser power increases, convection becomes dominant over conduction, resulting in vertically asymmetric diffraction ring patterns. In liquid media, when heat conduction dominates, the rings exhibit nearly perfect circular symmetry. In contrast, when vertical convection becomes stronger than conduction, the rings evolve into asymmetric circular patterns, with faster horizontal expansion than vertical expansion, leading to compression of the upper half of each ring relative to the horizontal direction. The formation dynamics of the diffraction rings can be described by an exponential model, $N = N_{max}(1-e^{t/\tau})$. Here, N is the number of diffraction rings, N_{max} is the maximum number of diffraction rings, and τ is the characteristic rise time for diffraction ring formation. Based on fitting with this exponential equation, τ is estimated to be 0.24 s at 532 nm and 0.38 s at 629 nm under the maximum laser intensity. The SSPM patterns generated by the MgB_2 nanosheets prepared in three different solvents (ethanol, N-Methyl-2-pyrrolidone, Dimethylformamide) have the following phenomena (Supporting information Figure S1). In three different solvents, the number of

Just Accepted

diffraction rings is the same, but their sharpness differs. The diffraction rings produced by the nanosheets in DMF and ethanol are clearer than those in NMP. The blurry fringes may resulted from the light scattering of nanosheets dispersion in NMP solvents[12]. In DMF solvent, the diffraction rings show good stability within 6 hours (Supporting information Figure S2).

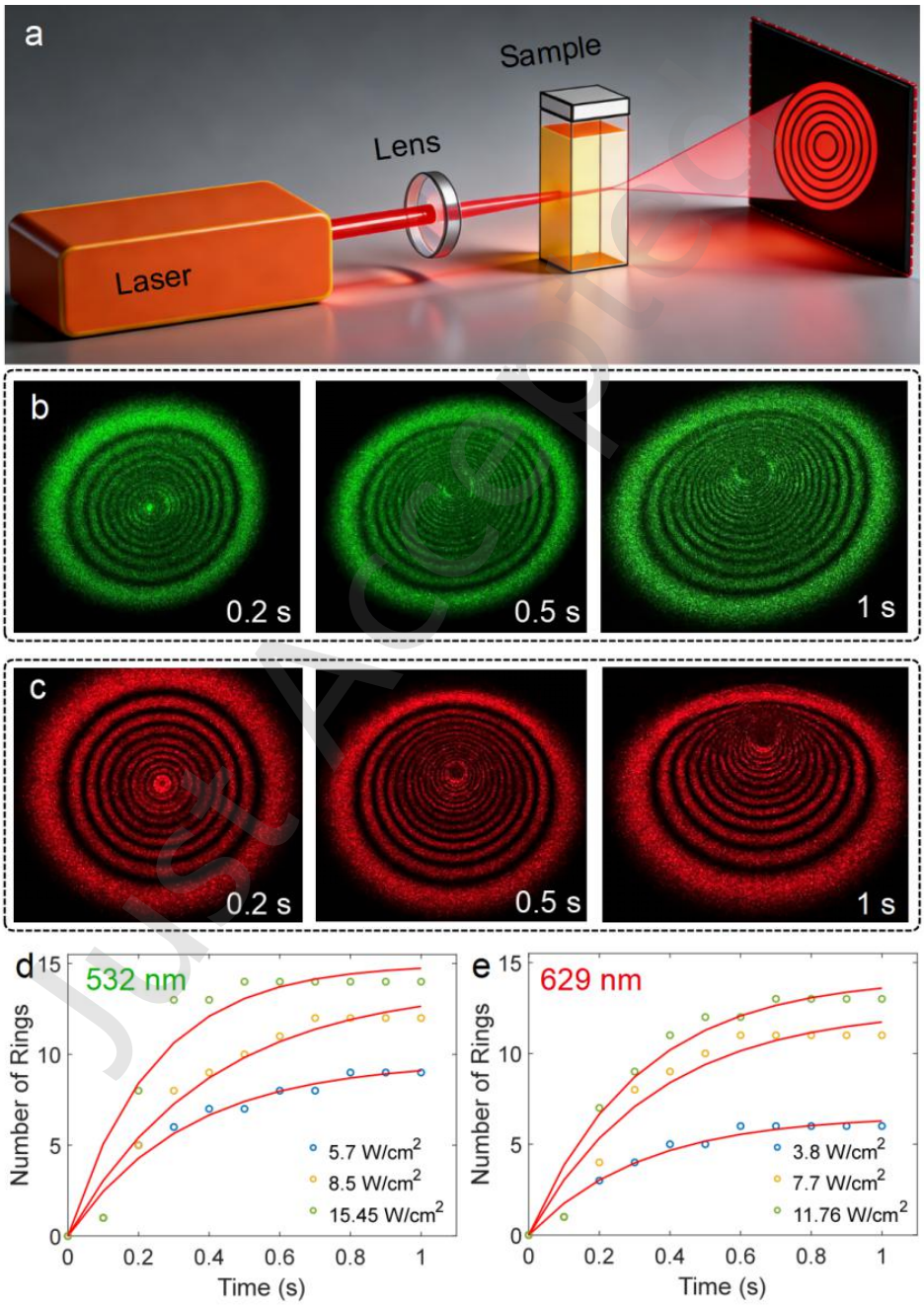


Figure 2 (a) Experimental setup for SSPM measurements based on MgB_2 nanosheet dispersions. (b, c) Temporal evolution of the diffraction ring patterns under laser excitation at wavelengths of 532 nm and 629 nm, respectively. (d, e) Time-dependent variation in the number of diffraction rings under different laser intensities at wavelengths of 532 nm and 629 nm, respectively.

Just Accepted

The diffraction ring patterns are sensitive to the incident laser intensity. As the laser intensity increases, a stronger nonlinear optical response is induced, leading to the generation of more diffraction rings. Figure 3a shows the intensity-dependent evolution of the diffraction ring patterns at wavelengths of 532 nm and 629 nm. With increasing optical intensity, the number of rings increases approximately linearly. In addition, higher input power results in an expansion of the ring pattern in both the horizontal and vertical directions. The nonlinear optical response R is defined as $R = N/I$, where I and N are the incident laser intensity and the number of diffraction rings, respectively. By fitting the experimental results shown in Figure 3c, the slope N/I can be extracted. The calculated R values of the MgB_2 nanosheet dispersion are 0.78 cm^2/W and 0.60 cm^2/W at 532 nm and 629 nm, respectively. The larger R value at 532 nm indicates a stronger nonlinear optical response compared with that at 629 nm. Based on these results, it is observed that the value of dN/dI rises as the wavelength of the incident laser increases. This wavelength-dependent behavior suggests that shorter-wavelength excitation, which carries higher photon energy, can induce a more pronounced SSPM response, consistent with previously reported results. The nonlinear refractive indices are estimated to be 1.41×10^{-9} m^2/W and 1.28×10^{-9} m^2/W at the wavelengths of 532 nm and 629 nm, respectively. The emergence of SSPM patterns is also influenced by several other factors, including the concentration of 2D materials dispersed in the solvent and the optical path length of the incident laser beam through the cuvette.

Just Accepted

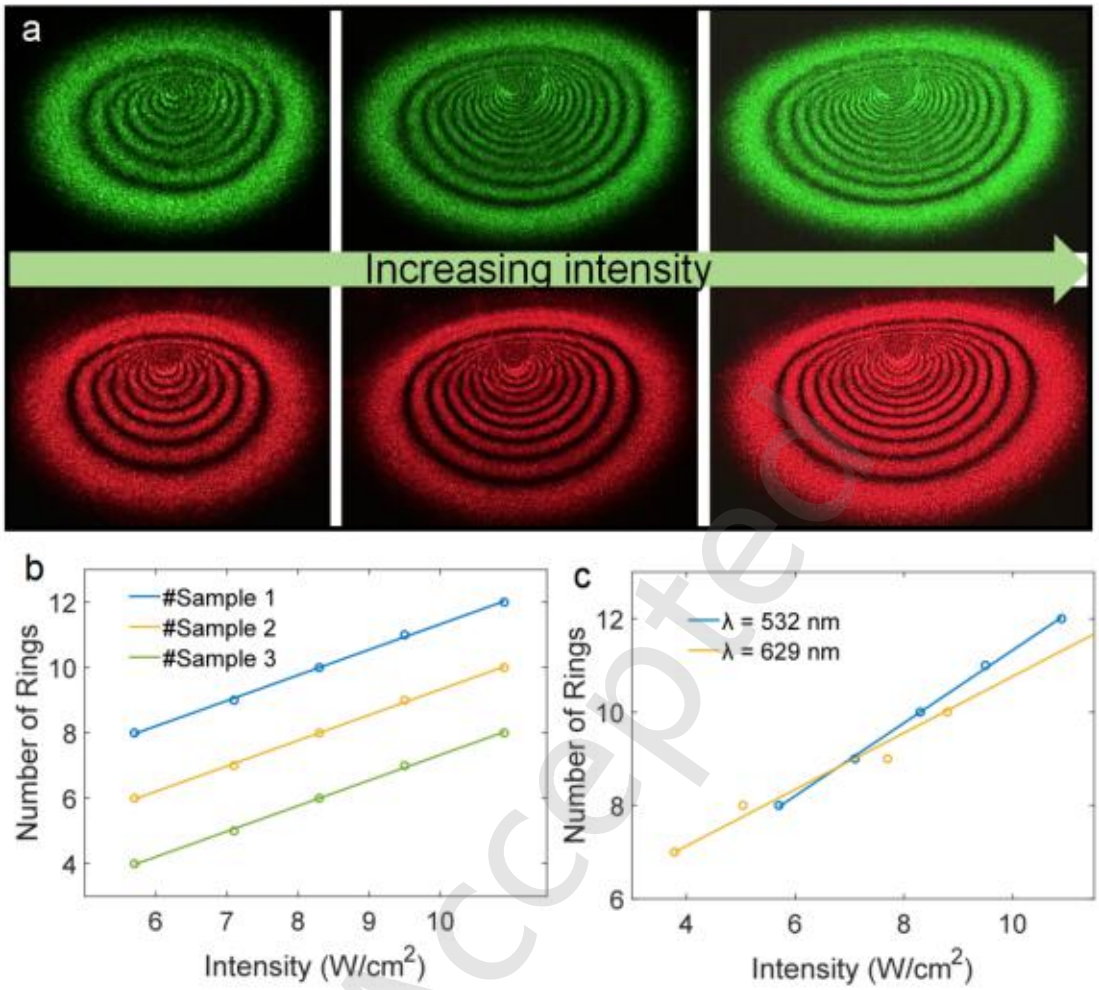


Figure 3. (a) Evolution of diffraction ring patterns with increasing laser intensity at wavelengths of 532 nm and 629 nm, respectively. (b, c) Variation in the number of diffraction rings as a function of incident laser intensity for MgB_2 nanosheet dispersions with different concentrations (#1 > #2 > #3) and under different excitation wavelengths of 532 nm and 629 nm, respectively.

3.4 All-optical switching based on MgB_2 nanosheets

In general, when two light beams intersect in a linear medium, they propagate independently without affecting each other. However, when the incident light is sufficiently intense, nanomaterials can absorb the laser energy and modulate the phase of the incident beam, thereby inducing SSPM. When two laser beams propagate simultaneously through a nanomaterial dispersion, their optical phases can be modulated through nonlinear light–matter interactions, giving rise to SXPM. Based on this effect, an all-optical switching scheme can be realized. Figure 4a illustrates the experimental setup for all-optical switching based on SXPM. In this configuration, a 532 nm green laser and a 629 nm red laser were used as the signal and control beams,

Just Accepted

respectively. Initially, the control and signal beams were combined using an optical beam splitter and then focused onto the MgB_2 nanosheet dispersion through a lens with a focal length of 200 mm. Initially, the intensities of both the 532 nm and 629 nm lasers were adjusted below the excitation threshold for SSPM, resulting in only laser spots without diffraction rings, as shown in Figure 4b. When the power of the control beam increases, diffraction ring patterns are generated by the coupled beams, as shown in Figure 4c. The number of diffraction rings increases with the improving control-beam intensity. Figure 4d shows the diffraction ring patterns obtained under different control-beam intensities. The ring number at 532 nm is larger than that at 629 nm, indicating a stronger nonlinear response at the shorter wavelength. The dependence of the signal beam diffraction ring number on the control-beam intensity is summarized in Figure 4(e). The extracted nonlinear optical response *R* of the signal beam is larger than that of the control beam, which is consistent with the experimental results shown in Figure 3c. According to the results in Figures 3 and 4, both single-wavelength excitation and simultaneous dual-wavelength excitation of the 2D MgB_2 can generate diffraction rings when the incident laser power exceeds the spatial self-phase modulation threshold, indicating that the "OR" logic gate function based on the diffraction rings is realized. To further demonstrate all-optical switching, an aperture was placed at the position of the outermost diffraction ring to selectively transmit light from a specific spatial region. A power meter was then used to measure the transmitted signal beam power as a function of the control-beam power, as shown in Figure 4f. As the control-beam power increases, the outermost bright ring first passes through the aperture, followed by a dark fringe. Consequently, the output power initially increases to a maximum and then decreases. The detected signal light power exhibits periodic oscillations with increasing control light power, confirming effective all-optical modulation. According to the formula (modulation depth = $10\log_{10}(P_{max}/P_{min})$) and time response curve, the maximum modulation depth (Figure 4f) and response time (Figure 2e) are 7.5 dB and ~0.3s, respectively. This behavior demonstrates the potential of MgB_2 nanosheets for all-optical switching applications,

Just Accepted

in which the signal light intensity can be modulated solely by changing the control light power. The switch is defined as being in the "ON" state when the detected signal power reaches a maximum and in the "OFF" state when the detected signal light power reaches a minimum.

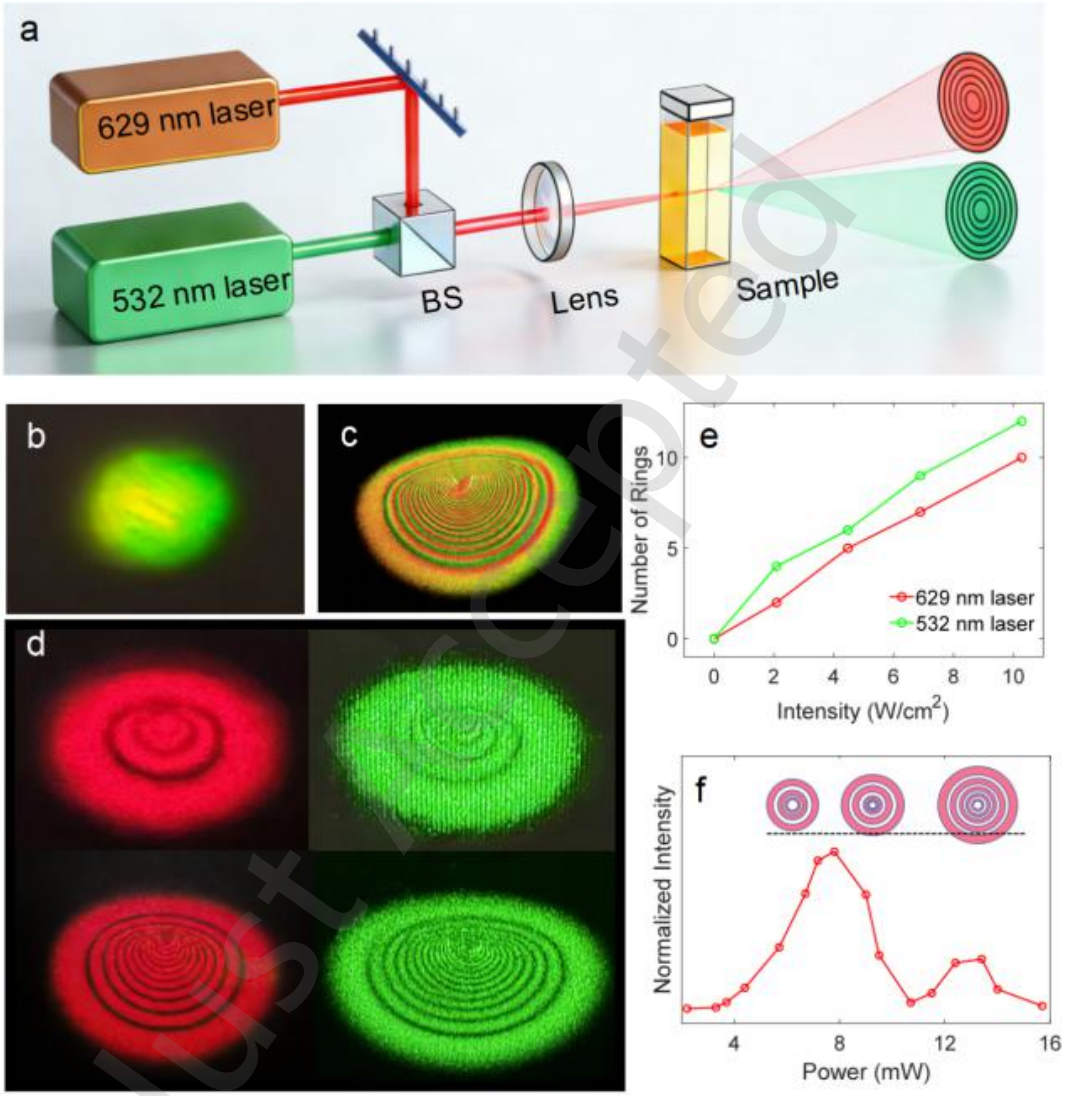


Figure 4. (a) Experimental setup for all-optical switching using MgB_2 nanosheet dispersions. (b, c, d) Light-field distributions after passing through the dispersion under different intensities of the 532 nm laser. (e) Variation in the number of diffraction rings as a function of red laser intensity for different laser wavelengths. (f) Demonstration of all-optical switching, in which the control light modulates the signal light to achieve ON/OFF switching states.

Just Accepted

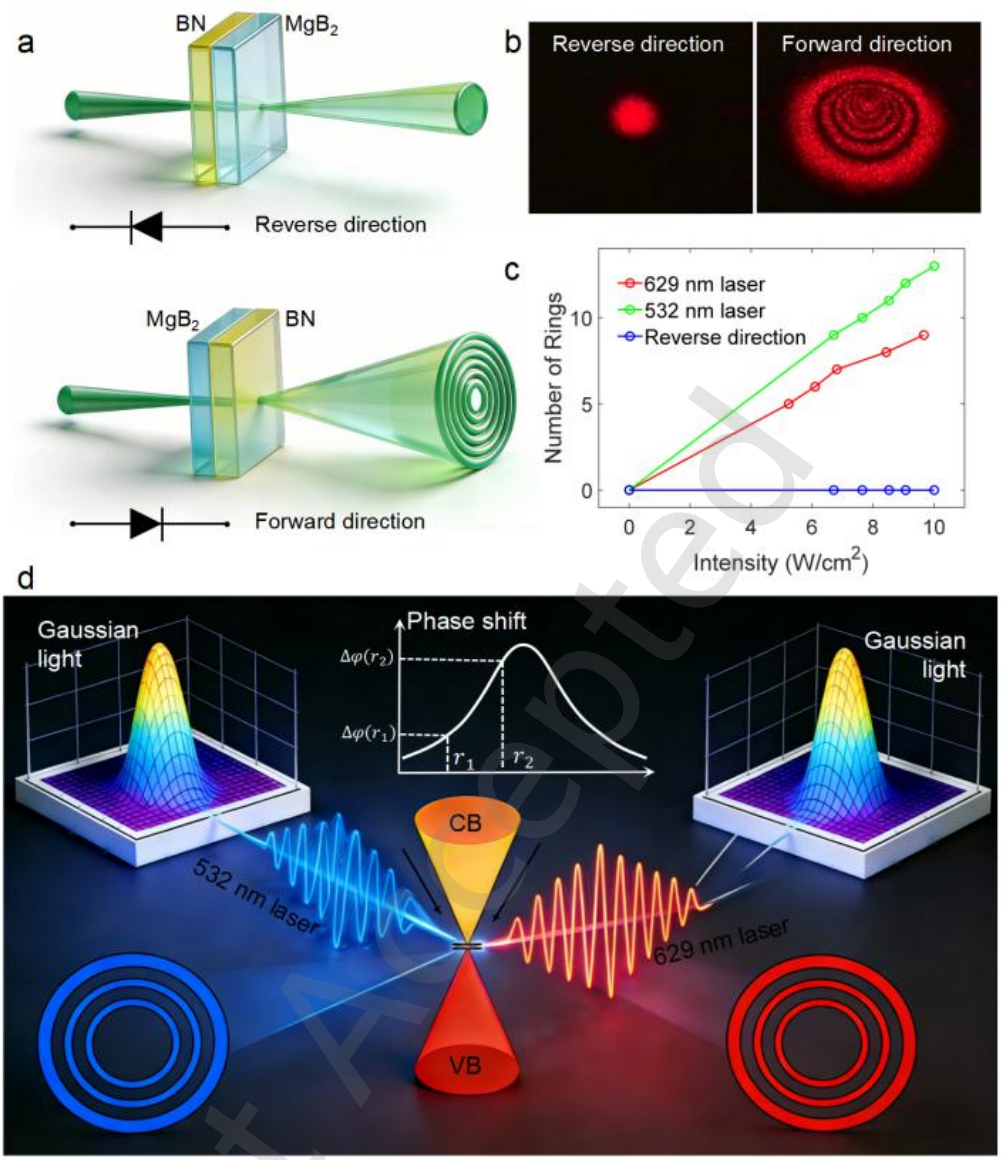


Figure 5. (a) Schematic illustration of the all-optical photonic diode based on the MgB_2/BN hybrid structure for achieving spatially asymmetric light propagation. (b) Diffraction ring patterns under reverse and forward propagation directions at a laser wavelength of 629 nm. (c) Variation in the number of diffraction rings as a function of laser intensity for different propagation directions and wavelengths. (d) Experimental schematic of SSPM based on 2D MgB_2 nanosheet dispersions.

3.5 Spatial asymmetric light propagation

In this section, nonreciprocal light propagation is demonstrated using a BN/MgB_2 hybrid structure to achieve spatially asymmetric light propagation. The hybrid configuration was constructed by placing two quartz cuvettes containing 2D MgB_2 and BN dispersions, respectively. When a 629 nm laser propagates in the forward direction (MgB_2→BN), the beam first interacts with the MgB_2 nanosheets, where the Kerr effect is excited and diffraction ring patterns are generated. The rings

Just Accepted

subsequently pass through the BN dispersion, where no additional rings are produced. Clear diffraction rings are observed in the forward propagation direction. In contrast, when the laser propagates in the reverse direction (BN→MgB_2), it first passes through the BN dispersion, where no diffraction rings are generated and the beam intensity is attenuated. Consequently, no diffraction rings are formed, and only a simple light spot is observed at the output. This asymmetric response, in which nonlinear excitation occurs only in one propagation direction, demonstrates the diode-like behavior of the 2D MgB_2/BN hybrid structure and highlights its potential for optical-isolator designs enabling spatially asymmetric light transmission. Notably, this unidirectional nonlinear effect is not limited to 629 nm excitation but is also observable at 532 nm, indicating the broadband capability of the hybrid structure for direction-dependent light propagation. The detailed evolution of the diffraction rings in the nonlinear photonic diode under forward and reverse propagation is shown in Figure 5c. The nonlinear optical response at 532 nm is stronger than that at 629 nm, which is consistent with the SSPM results.

The experimental setup employs laser sources at 532 nm and 629 nm, both of which have photon energies sufficient to induce electronic transitions in MgB_2 nanosheets. Under laser irradiation, electrons can be excited from the valence band (VB) to the conduction band (CB), as illustrated in Figure 5d, owing to strong light-matter interaction within the MgB_2 dispersion. As the laser beam propagates through the dispersion, the Kerr nonlinearity of the 2D MgB_2 nanosheets is activated. The incident beam has a Gaussian intensity profile, with the highest intensity at the center and a gradual decrease toward the periphery. Because the 2D MgB_2 nanosheets act as an intensity-dependent nonlinear medium, this spatially varying intensity distribution across the Gaussian beam induces a corresponding phase-shift ($\Delta\varphi$) profile upon transmission, which itself assumes a Gaussian-like form. Within this phase-shift distribution, two radial positions, r_1 and r_2, can possess identical local slopes, indicating equal wave vectors ($(d\Delta\varphi/dr)$ evaluated at r_1 equals that at r_2). This condition enables optical interference between light components originating from

Just Accepted

these two positions. The phase difference between these two points satisfies $\Delta\varphi(r_1) - \Delta\varphi(r_2) = M\pi$, where M is an integer. Even and odd values of M correspond to constructive and destructive interference, respectively, giving rise to bright and dark concentric fringes. Consequently, a distinct diffraction ring pattern is formed on a screen placed behind the sample, corresponding to the well-documented phenomenon of SSPM. If a Gaussian beam is modulated into other modes, the diffraction ring pattern will also change (Supporting information Figure S3). Excitation of different optical field modes will produce different output optical fields. The optical field patterns are relatively complex and various, which provides a novel view for realizing optical switching of transverse optical fields.

Just Accepted

Conclusion

This study investigates 2D MgB_2 as an emerging nonlinear optical material with promising potential for nonlinear photonic devices. The experimental results reveal that 2D MgB_2 nanosheets exhibit a strong nonlinear optical response, making them attractive candidates for advanced nonlinear optical components, including optical diodes, all-optical switches, and optical modulators. The nonlinear refractive index (n_2) was quantitatively evaluated to be 1.41×10^{-9} m^2/W and 1.28×10^{-9} m^2/W at excitation wavelengths of 532 nm and 629 nm, respectively. By leveraging the strong Kerr nonlinearity of 2D MgB_2, a MgB_2/BN nanosheet hybrid architecture was developed to realize nonreciprocal light transmission, demonstrating its functionality as a nonlinear photonic diode. In addition, a light-controlled light modulation system based on 2D MgB_2 was designed for all-optical switching applications. In this system, a high-power control beam modulates a low-power signal beam through SXPM, enabling reversible switching between "ON" and "OFF" states. The successful implementation of 2D MgB_2 nanosheets in photonic diodes and all-optical modulators highlights their significant potential for applications in nonlinear optics and integrated photonic devices.

Just Accepted

Acknowledgements

This work was financially supported by Shenzhen Science and Technology Program (QNXMC20250701091303006), Faculty Pioneering Team Initiative (202504097333), Youth Innovation Talent Program of Guangdong Province (2025KQNCX164), Youth S&T Talent Support Programme of Guangdong Provincial Association for Science and Technology (GDSTASKXRC2026871) and other program (SUIT2026KJ015, SZIIT2025KJ069). C.Tan thanks the funding support from the Start-Up Grant (Project No. 9610710) from City University of Hong Kong and ITC via Hong Kong Branch of National Precious Metals Material Engineering Research Center (NPMM).

Declaration of competing interest The authors declare that they have no known competing financial interests or personal relationships that could have appeared to influence the work reported in this paper.

4. References

[1] Liao, K.; Chen, Y.; Yu, Z.; Hu, X.; Wang, X.; Lu, C.; Lin, H.; Du, Q.; Hu, J.; Gong, Q. All-optical computing based on convolutional neural networks. *Opto-Electron. Adv*. **2021**, *4*, 200060.

[2] Paredes-Barato, D.; Adams, C. S. All-optical quantum information processing using rydberg gates. *Phys. Rev. Lett*. **2014**, *112*, 040501.

[3] Wang, C.; Chen, Q.; Chen, H.; Liu, J.; Song, Y.; Liu, J.; Li, D.; Ge, Y.; Gong, Y.; Zhang, Y.; Zhang, H. Boron quantum dots all-optical modulator based on efficient photothermal effect. *Opto-Electron. Adv*. **2021**, *4*, 200032.

[4] Wang, C.; Xu, J.; Wang, Y.; Song, Y.; Guo, J.; Huang, W.; Ge, Y.; Hu, L.; Liu, J.; Zhang, H. MXene (Ti_2NT_x): Synthesis, characteristics and application as a thermo-optical switcher for all-optical wavelength tuning laser. *Sci. China Mater*. **2020**, *64*, 259-265.

[5] Wu, Y.; Wu, Q.; Sun, F.; Cheng, C.; Meng, S.; Zhao, J. Emergence of electron coherence and two-color all-optical switching in MoS_2 based on spatial self-phase modulation. *Proc. Natl. Acad. Sci. U.S.A*. **2015**, *112*, 11800-11805.

[6] Xu, J.; Zhang, C.; Wang, Y.; Wang, M.; Xu, Y.; Wei, T.; Xie, Z.; Liu, S.; Lee, C.-K.; Hu, X.; Zhao, G.; Lv, X.; Zhang, H.; Zhu, S.; Zhou, L. All-in-one, all-optical logic gates using liquid metal plasmon nonlinearity. *Nat. Commun*. **2024**, *15*, 1726.

[7] Xiao, S.; Ma, Y.; He, Y.; Wang, Y.; Xin, H.; Fan, Q.; Zhang, J.; Li, X.; Zhang, Y.; He, J.; Wang, Y. Revealing the intrinsic nonlinear optical response of a single MoS_2 nanosheet in a suspension based on spatial self-phase modulation. *Photonics Res*. **2020**, *8*, 1725-1733.

[8] Wu, L.; Fan, T.; Wei, S.; Xu, Y.; Zhang, Y.; Ma, D.; Shu, Y.; Xiang, Y.; Liu, J.; Li, J.; Panajotov, K.; Qin, Y.; Zhang, H. All-optical logic devices based on black arsenic–phosphorus with strong nonlinear optical response and high stability. *Opto-Electron. Adv*. **2022**, *5*, 200046.

[9] Xu, X.; Wang, M.; Zhang, Y.; Li, Q.; Niu, W.; Yang, Y.; Zhao, J.; Wu, Y. Broadband spatial self‐phase modulation in black and violet phosphorus and near‐infrared all‐optical switching. *Laser Photonics Rev*. **2023**, *18*, 2300930.

[10] Wu, L.; Jiang, X.; Zhao, J.; Liang, W.; Li, Z.; Huang, W.; Lin, Z.; Wang, Y.; Zhang, F.; Lu, S.; Xiang, Y.; Xu, S.; Li, J.; Zhang, H. MXene‐based nonlinear optical information converter for all‐optical modulator and switcher. *Laser Photonics Rev*. **2018**, *12*, 1800215.

[11] Goswami, S.; de Oliveira, C. C.; Ipaves, B.; Mahapatra, P. L.; Pal, V.; Sarkar, S.; Autreto, P. A. S.; Ray, S. K.; Tiwary, C. S. Exceptionally high nonlinear optical response in two‐dimensional type II dirac semimetal nickel di‐telluride ($NiTe_2$). *Laser Photonics Rev*. **2025**, *19*, 2400999.

[12] Gao, Y.; Ling, C.; Weng, D.; Rui, G.; He, J.; Gu, B. Demonstration of spatial asymmetric light propagation performance Using violet phosphorus quantum dots with tunable bandgap. *Laser Photonics Rev*. **2024**, *18*, 2301062.

[13] Dey, P.; Pal, P.; Das, B. K.; Bhattacharjee, S.; Chakraborty, N.; Das, B.; Ruidas, S.; Chattopadhyay, K. K. High nonlinear optical response of covalent organic framework by SSPM for implementation in photonic diode. *Laser Photonics Rev*. **2026**, *20*, e02455.

[14] Ji, W.; Chen, W.; Lim, S.; Lin, J.; Guo, Z. Gravitation-dependent, thermally-induced selfdiffraction in carbon nanotube solutions. *Opt. Express* **2006**, *14*, 8958-8966.

[15] Wu, R.; Zhang, Y.; Yan, S.; Bian, F.; Wang, W.; Bai, X.; Lu, X.; Zhao, J.; Wang, E. Purely

Just Accepted

coherent nonlinear optical response in solution dispersions of graphene sheets. *Nano Lett*. **2011**, *11*, 5159-5164.

[16] Wang, G.; Zhang, S.; Umran, F. A.; Cheng, X.; Dong, N.; Coghlan, D.; Cheng, Y.; Zhang, L.; Blau, W. J.; Wang, J. Tunable effective nonlinear refractive index of graphene dispersions during the distortion of spatial self-phase modulation. *Appl. Phys. Lett*. **2014**, *104*, 141909.

[17] Wu, L.; Dong, Y.; Zhao, J.; Ma, D.; Huang, W.; Zhang, Y.; Wang, Y.; Jiang, X.; Xiang, Y.; Li, J.; Feng, Y.; Xu, J.; Zhang, H. Kerr nonlinearity in 2D graphdiyne for passive photonic diodes. *Adv. Mater*. **2019**, *31*, 1807981.

[18] Ge, Y.; Wang, W.; Wang, M.; Zhang, S.; Zhong, Y.; Zhang, Y.; Wei, S.; Du, B.; Wang, H.; Qiu, M.; Liu, G.; Zhang, L.; Li, J.; Yue, Y.; Zhang, H. All-optical logic processing unit using Kerr nonlinearity of MXene. *Nat. Commun*. **2026**, *17*, 4078.

[19] Yi, J.; Li, J.; Huang, S.; Hu, L.; Miao, L.; Zhao, C.; Wen, S.; Mochalin, V. N.; Rao, A. M. Ti_2CT_x MXene‐based all‐optical modulator. *InfoMat* **2019**, *2*, 601-609.

[20] X. Zeng, A. V. Pogrebnyakov, A. Kotcharov, J. E. Jones, X. X. Xi, E. M. Lysczek, J. M. Redwing, S. Xu, Q. Li, J. Lettieri, D. G. Schlom, W. Tian, X. Pan and Z. K. Liu. In situ epitaxial MgB_2 thin films for superconducting electronics. *Nature Materials*. 2002: **1**, 1-4.

[21] Eom, C. B.; Lee, M. K.; Choi, J. H.; Belenky, L. J.; Song, X.; Cooley, L. D.; Naus, M. T.; Patnaik, S.; Jiang, J.; Rikel, M.; Polyanskii, A.; Gurevich, A.; Cai, X. Y.; Bu, S. D.; Babcock, S. E.; Hellstrom, E. E.; Larbalestier, D. C.; Rogado, N.; Regan, K. A.; Hayward, M. A.; He, T.; Slusky, J. S.; Inumaru, K.; Haas, M. K.; Cava, R. J. High critical current density and enhanced irreversibility in superconducting MgB_2 thin films. *Nature* **2001**, *411*, 558-560.

[22] Choi, H. J.; Roundy, D.; Sun, H.; Cohen, M. L.; Louie, S. G. The origin of the anomalous superconducting properties of MgB_2. *Nature* **2002**, *418*, 458-460.

[23] Larbalestier, D. C.; Cooley, L. D.; Rikel, M. O.; Polyanskii, A. A.; Jiang, J.; Patnaik, S.; Cai, X. Y.; Feldmann, D. M.; Gurevich, A.; Squitieri, A. A.; Naus, M. T.; Eom, C. B.; Hellstrom, E. E.; Cava, R. J.; Regan, K. A.; Rogado, N.; Hayward, M. A.; He, T.; Slusky, J. S.; Khalifah, P.; Inumaru, K.; Haas, M. Strongly linked current flow in polycrystalline forms of the superconductor MgB_2. *Nature*. **2001**, *410*, 186-189.

[24] Bugoslavsky, Y.; Cohen, L. F.; Perkins, G. K.; Polichetti, M.; Tate, T. J.; Gwilliam, R.; Caplin, A. D. Enhancement of the high-magnetic field critical current density of superconducting MgB_2 by proton irradiation. *Nature* **2001**, *411*, 561-563.

[25] Kang, W. N.; Kim, H.-J.; Choi, E.-M.; Jung, C. U.; Lee, S.-I. MgB_2 superconducting thin films with a transition temperature of 39 kelvin. *Science* **2001**, *292*, 1521-1523.

[26] Dahm, T.; Scalapino, D. J. Nonlinear microwave response of MgB_2. *Appl. Phys. Lett*. **2004**, *85*, 4436-4438.

[27] Cheng, S. H.; Zhang, Y.; Wang, H. Z.; Li, Y. L.; Yang, C.; Wang, Y. Fabrication and characterization of superconducting MgB_2 thin film on graphene. *AIP Adv*. **2018**, *8*, 075015.

[28] Yuan, J.; Shi, L.; Xu, T.; Wang, Y.; Gan, Z.; Wang, H.; Wu, T.; Wu, D.; Dong, T.; Wang, N. Selective excitation of collective modes in multiband superconductor MgB_2. *Phys. Rev. Lett*. **2025**, *135*, 166022.

[29] Shibata, H. Fabrication of a MgB_2 nanowire single-photon detector using Br_2–N_2dry etching. *Appl. Phys. Express*. **2014**, *7*, 103101.

[30] Novoselov, E.; Cherednichenko, S. Low noise terahertz MgB_2 hot-electron bolometer mixers with an 11 GHz bandwidth. *Appl. Phys. Lett*. **2017**, *110*, 032601.

Just Accepted

[31] Charaev, I.; Batson, E. K.; Cherednichenko, S.; Reidy, K.; Drakinskiy, V.; Yu, Y.; Lara-Avila, S.; Thomsen, J. D.; Colangelo, M.; Incalza, F.; Ilin, K.; Schilling, A.; Berggren, K. K. Single-photon detection using large-scale high-temperature MgB_2 sensors at 20 K. *Nat. Commun.* **2024**, *15*, 3973.

[32] Shibata, H.; Maruyama, T.; Akazaki, T.; Takesue, H.; Honjo, T.; Tokura, Y. Photon detection and fabrication of MgB_2 nanowire. *Phys. C: Supercond. Appl.* **2008**, *468*, 1992-1994.

[33] Morshed, M.; Hattori, H. T.; Haque, A.; Olbricht, B. C. Magnesium diboride (MgB_2) as a saturable absorber for a ytterbium-doped Q-switched fiber laser. *Appl. Optics* **2017**, *56*, 7611.

[34] Li, W. X.; Li, Y.; Chen, R. H. R.; Zhu, Y.; Jin H. M.; Dou, S. X. Electron–phonon coupling properties in MgB_2 observed by Raman scattering. *J. Phys. Condens. Matter* **2008**, *20*, 255235.

[35] Talapatra, A.; Bandyopadhyay, S. K.; Sen, P.; Barat, P.; Mukherjee, S.; Mukherjee, M. X-ray photoelectron spectroscopy studies of MgB_2 for valence state of Mg. *Phys. C: Supercond. Appl.* **2005**, *419*, 141-147.

[36] Li, J.; Zhang, Z.; Yi, J.; Miao, L.; Huang, J.; Zhang, J.; He, Y.; Huang, B.; Zhao, C.; Zou, Y.; Wen, S. Broadband spatial self‐phase modulation and ultrafast response of MXene $Ti_3C_2T_x$ (T=O, OH or F). *Nanophotonics* **2020**, *9*, 2415-2424.

[37] Wu, L.; Chen, K.; Huang, W.; Lin, Z.; Zhao, J.; Jiang, X.; Ge, Y.; Zhang, F.; Xiao, Q.; Guo, Z.; Xiang, Y.; Li, J.; Bao, Q.; Zhang, H. Perovskite $CsPbX_3$: A promising nonlinear optical material and its applications for ambient all‐optical switching with enhanced stability. *Adv. Opt. Mater.* **2018**, *6*, 1800400.

Just Accepted

Electronic Supplementary Material

All-optical modulator and switcher based on 2D MgB_2 nanosheets with strong nonlinear optical response

Cong Wang [1], Xiangrong Pan [2], Jiajia Zha [3], Yichao Bai [4], Chunjiang Li [4], Kaichen Dong [4], Dan Liu [1], Shiguo Li [1], Yu Lei [4], Zhan Zhou [2], Han Zhang [5], Chaoliang Tan [3,6] ✉

[1] School of Microelectronics, Shenzhen University of Information Technology, Shenzhen 518172, China
[2] College of Chemistry and Chemical Engineering, Luoyang Normal University, Luoyang 471934, China
[3] Department of Electrical Engineering, City University of Hong Kong, Kowloon Tong, Hong Kong SAR 999077, China
[4] Institute of Materials Research, Shenzhen Key Laboratory of Advanced Layered Materials for Value-added Applications, Institute of Data and Information, Center of Double Helix, Tsinghua Shenzhen International Graduate School, Tsinghua University, Shenzhen 518055, China
[5] Collaborative Innovation Center for Optoelectronic Science & Technology, International Collaborative Laboratory of 2D Materials for Optoelectronics Science and Technology of Ministry of Education, Institute of Microscale Optoelectronics, Shenzhen University, Shenzhen 518060, China
[6] Department of Biomedical Engineering and Hong Kong Branch of National Precious Metals Material Engineering Research Center (NPMM), City University of Hong Kong, Kowloon Tong, Hong Kong SAR 999077, China

✉ Address correspondence to Chaoliang Tan, chaoltan@cityu.edu.hk

Supporting information to https://doi.org/10.26599/NR.2026.94909312

Just Accepted

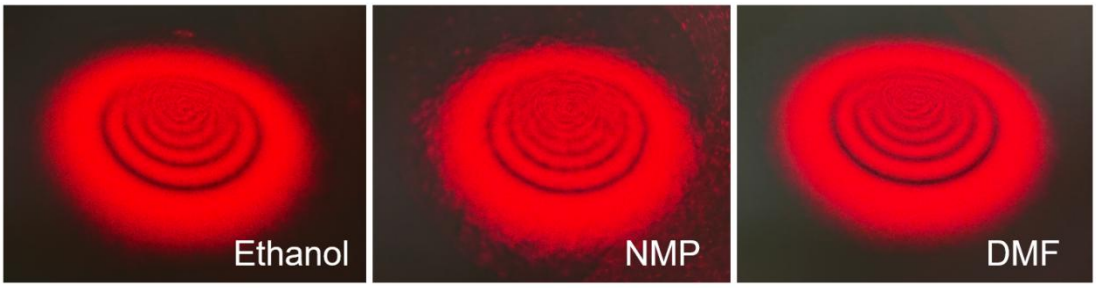


Figure S1. Diffraction ring patterns of different solvents: ethanol, N-Methyl-2-pyrrolidone (NMP), Dimethylformamide (DMF).

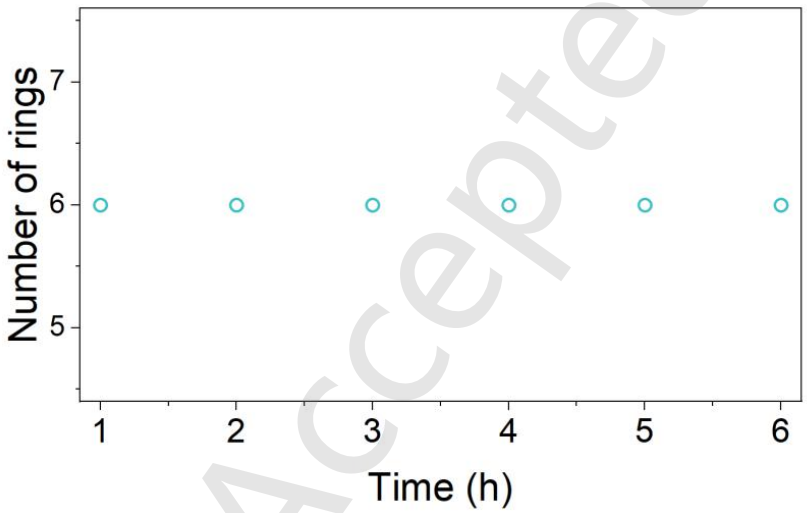


Figure S2. The variation of diffraction rings with time.

Just Accepted

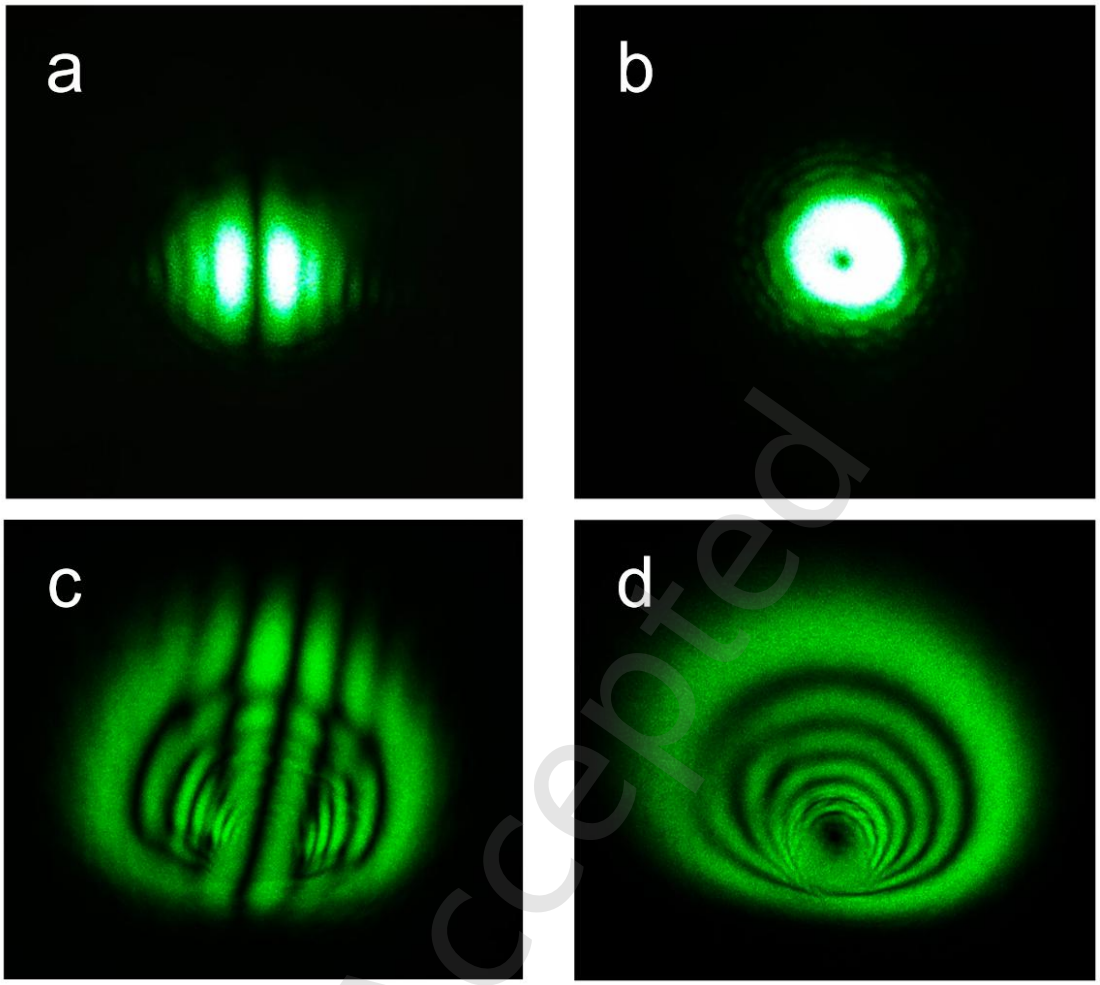


Figure S3. Diffraction ring patterns under the different excitation laser mode. Under (a) Hermite-Gaussian light field and (b) Laguerre-Gaussian light field excitation, the output light fields (c) and (d) were obtained, respectively. The Hermite-Gaussian and Laguerre-Gaussian were generated by phase plate.

Just Accepted